Low-Cost and Low-Profile Sub-Terahertz Luneburg Lens Beamformer on Polymer

Adham Mahmoud, Jorge Ruiz-Garcia, Olivier de Sagazan, Mauro Ettorre, Ronan Sauleau, David Gonzalez-Ovejero

Low-Cost and Low-Profile Sub-Terahertz Luneburg Lens Beamformer on Polymer

Adham Mahmoud, Jorge Ruiz-García, Olivier de Sagazan, Mauro Ettorre, *Fellow, IEEE*, Ronan Sauleau, *Fellow, IEEE*, David González-Ovejero, *Senior Member, IEEE*

***Abstract*—A Luneburg lens is used to excite a leaky-wave antenna (array of slots) in the sub-terahertz (sub-THz) frequency range. The antenna is built on a 140-µm thick Cyclic Olefin Copolymer (COC) substrate. The radiating slots (58×24 slots) are etched on the polymer by a photolithographic process, for which the gold (Au) layers are first deposited by evaporation on the COC and, then, patterned by chemical etching. No metalized vias or drilling are applied to the substrate. The full system is fed by a standard WR03 waveguide, and it has been fabricated and tested. Experimental results show an input reflection coefficient better than −7 dB over a 25% fractional bandwidth, spanning from 220 GHz to 290 GHz. The radiated beam can be steered in elevation from -80° to -20° over the same band. The antenna efficiency is estimated to be 20% at the center frequency (260 GHz). This solution provides a simple alternative for low-cost and low-profile beam scanning antennas in the sub-THz range.**

***Index Terms*—Beam-formers, COC, leaky-wave antennas, Luneburg lens, polymers.**

I. Introduction

SUB-TERAHERTZ (sub-THz) frequencies have been identified as very promising to provide data rates exceeding 100 Gb/s [1] in 6G and beyond wireless systems [2]-[3]. However, directive pencil-beam antennas must be used in this frequency range to compensate for the high free-space path loss (FSPL) and atmospheric absorption. Such high gains may be obtained with reflectors or lenses; but these structures are too bulky for indoor systems and not suitable for a massive deployment as foreseen in future wireless networks [3]. Beam-steering is also compulsory to accurately align antennas with narrow beam-width in long-distance point-to-point links [4] and to enable user mobility and point-to-multipoint operation [5]. Leaky-wave antennas (LWA) [6] are a simple solution to steer a beam without the need of phase shifters [7] by just using a different carrier frequency. As a result, low-profile LWA architectures based on low-cost organic materials and fabrication techniques are a promising solution to satisfy the stringent tolerances and to overcome losses at such high frequencies.

Computer numerical control (CNC) milling [8]-[9], deep reactive ion etching (DRIE) [10]-[12] or diffusion bonding [13] are rising technologies to manufacture structures based on hollow waveguides that maximize the radiation efficiency [14]. However, such solutions may lead to costly and bulky systems. As an alternative, substrate integrated waveguide (SIW) technology are used under 200 GHz to reduce the costs and simplify the fabrication. If the required design frequency is higher, this would require metallized vias with a diameter smaller than 50 µm, which adds complexity to the fabrication procedure and increases its cost, similar to the air-based systems [15]. Moreover, selecting the appropriate materials with moderate losses is crucial for SIW to avoid a negative impact on the total efficiency of the radiating system. Polymer substrates are known for their low dielectric constant and low losses at high frequencies [16]-[17]. Nevertheless, their low glass transition temperature (T_g) prevents the use of SIW technology, since the high-temperature steps required for laser drilling and metallizing the substrate will damage the polymer.

This work addresses some of the aforementioned problems by presenting the design of a low-profile LWA system on a low-loss polymer substrate: Cyclic Olefin Copolymer (COC). In this paper, a low-loss high-gain polymer-based antenna is presented. The antenna is fabricated through a simple explained procedure. No drilled vias are required at all at any part of the system to further simplify the fabrication. The proposed antenna system is made of two building blocks, as shown in Fig. 1, namely: a quasi-optical beam former based on a flat Luneburg lens and an array of slots. The Luneburg lens transforms the cylindrical wave coming from the antenna feeder to a plane wave that illuminates the array of slots. This array is located on the same substrate as the quasi-optical beam former and operates as a LWA with frequency-controlled beam scanning. The radiating aperture of the array is tapered to increase the aperture efficiency. SIW and drilling/via holes are avoided in the structure to enable fabrication. The system is very cheap and simple compared to other fabrication technologies at the same frequency bands.

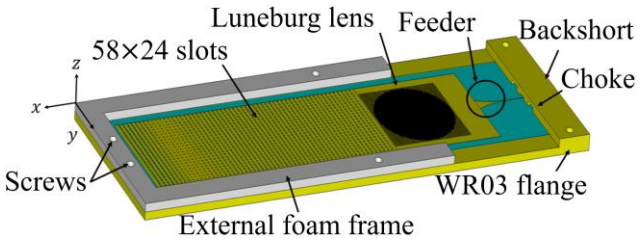

Fig. 1. 3D perspective view of the proposed antenna system.

II. Antenna Configuration

The proposed antenna has been designed on a COC substrate, commercially known as Topas 8007 ($\epsilon_r = 2.2, \tan\delta = 0.002$ at 300 GHz) [17]. It can be divided in two main building blocks: the Luneburg lens and the leaky-wave antenna made by an array of slots. The whole system is placed above an aluminum supporting interface for testing. This interface is also described in the following, and its impact on the antenna performance commented.

II. A) Flat Luneburg lens

The lens is fed by an exponentially tapered transmission line, which acts as primary source. The exponential taper of the source is engineered to launch a transverse electromagnetic (TEM) mode within the substrate. Such a mode presents a cylindrical wavefront and provides a field tapering of −13 dB over the lens's edge. The Luneburg lens converts the cylindrical wavefront into a planar one, which illuminates the radiating slots. The lens diameter is 10 mm (or $14\lambda_g$, with λ_g being the guided wavelength in the substrate at 260 GHz). The distance between the lens center and the phase center of the feeder is 10.3 mm ($11.5\lambda_g$). The resulting modified Luneburg lens presents a refractive index profile *n* given by:

$$n(r) \approx \left[1+\sqrt{1-\left(\frac{nr}{d}\right)^2}\right]^{\frac{1}{2}} \exp\left(-\frac{1}{\pi}\int_1^a \frac{\sin^{-1}\left(\frac{t}{d}\right)}{\sqrt{t^2-(nr)^2}}dt\right), \quad (1)$$

where d is the normalized distance between the phase center of the feeder and the center of the lens [18], r is the distance between a point in the lens and its center, and a is the lens radius. According to (1), the maximum required refractive index is 2.1 at the lens center if the phase center is located at the rim of the lens. In our case, a gap of $2\lambda_g$ is left between the phase center of the feeder and the periphery of the lens. This choice will reduce the maximum required refractive index at the center of the lens from 2.1 to 1.85, simplifying its implementation. The refractive index required for the lens then ranges from 1.48 to 1.85.

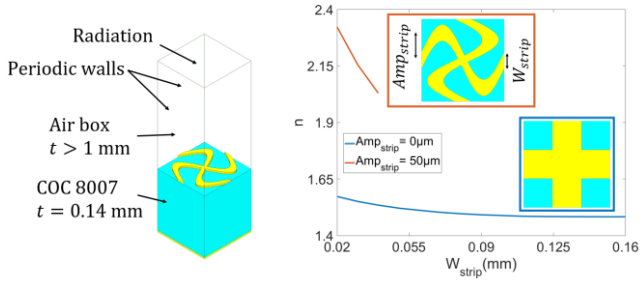

(a) (b)

Fig. 2. Unit-cell of the Luneburg lens. (a) Perspective view. (b) Retrieved refractive index at 260 GHz versus strip width and for two strip amplitudes (Amp_{strip} = 0 μm and Amp_{strip} = 50 μm).

A grid of crossed sinusoidal-shaped transmission lines is adopted to synthetize the required refractive index profile. The unit-cell is presented in Fig. 2 (a). Its periodicity is approximately $0.2\lambda_g$ (0.16 mm). Once the periodicity has been fixed, the refractive index of the unit-cell can be controlled by tuning the width of the strip W_{strip} and its amplitude Amp_{strip} [19]. The maximum amplitude of the strip considered in the optimization process is 50 μm. The resulting refractive index is reported in Fig. 2 (b) as a function of W_{strip}. From Fig. 2 (b), it can be noticed that the minimum achievable refractive index is equal to 1.48, which corresponds to the supporting material of the parallel plate waveguide (PPW) structure. Reducing the width of the transmission line and increasing its sinusoidal amplitude leads to an increase in the calculated refractive index up to 2.36. It should be noted that increasing the sinusoidal amplitude imposes a constraint on the realization of such a feature inside the unit cell with a size of $0.2\lambda_g$. A full database is built by interpolating the refractive index values for different strip amplitudes (Amp_{strip}) varying from 0 μm (non-modulated transmission line) to 50 μm with a 5 μm step, and strip widths (W_{strip}) from 20 to 160 μm with a 1 μm step. Next, the lens circular area is discretized according to a Cartesian lattice that matches the side of our unit-cell. Finally, the geometries of the unit-cells constituting our lens are retrieved by interpolation from the aforementioned database.

II. B) Leaky-wave antenna

The second block of the antenna is the radiating aperture composed by an array of slots (see Fig. 1) operating as a leaky-wave antenna. The periodicity of the slots is 0.53 mm and 0.51 mm along *x* and *y* respectively, as illustrated in Fig. 1. The array comprises 58 slots along *x* and the lens diameter allows to accommodate 24 slots along *y*. For a plane TEM mode illuminating the array along *x*, the direction of the radiated beam is dictated by the periodicity along *x* (P_x) yielding

$$\sin\theta_m = \lambda_0(1/\lambda_g - 1/P_x), \quad (2)$$

where θ_m is the pointing angle of the main beam, λ_0 is the wavelength in free space and λ_g is the guided wavelength [20]. Substituting $P_x = 0.53$ mm into (2) leads to a scanning angle θ_m equal to 30° in the backward quadrant at 260 GHz. Aperture tapering is applied to reach a uniform power distribution across the slots to maximize its aperture efficiency [20]. A parametric sweep on the length of the slot has been applied to link the radiated power to the slot length (Fig. 3 (a)). By modulating the slot lengths, a 99% of the power is radiated by the antenna. The slot lengths are plotted against their positions in the array in Fig. 3 (b).

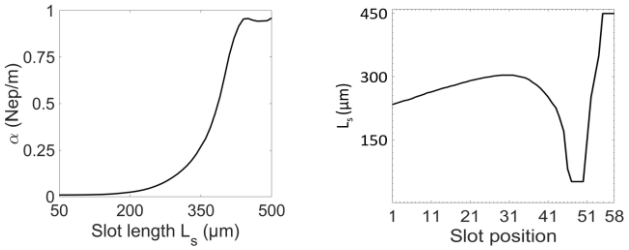

(a) (b)

Fig. 3. Details of the slot array. (a) Slot length versus leakage rate. (b) Slot length versus position along the *x* axis.

II. C) Supporting block

The whole antenna system is mounted on a supporting block for testing and feeding. In particular, a standard WR03 waveguide (0.864×0.432 mm^2) is used to feed the full antenna. A transition from the standard waveguide to the flared transmission line feeding the Luneburg lens has been designed (Fig. 4 (a)).

This transition can be divided into 3 main parts: back short, main waveguide feeder, and a fan-shaped probe etched on top of the substrate. The soft nature of the COC polymer prevents fabrication of metallized via holes. Instead, the back-short and the main feeder include chokes to minimize power leakage.

The transition has been simulated using CST Studio Suite [21]. The results are plotted in Fig. 4 (b). The transition shows a wide band operation that extends from 220 GHz to 290 GHz with a reflection coefficient better than −12.5 dB, and insertion losses lower than 2.5 dB in the same band.

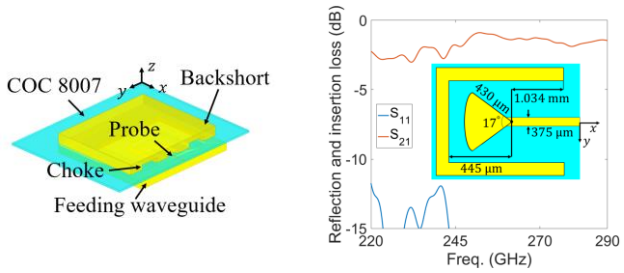

(a) (b)

Fig. 4. Transition from standard rectangular waveguide (WR03) to the primary feed. (a) Perspective view. (b) Dimensions of the transition and simulated magnitude of the input reflection coefficient (S_{11}) and transmission coefficient (S_{21}) in dB.

III. Numerical Results

The antenna system represented in Fig. 1 has been simulated using CST Studio Suite. Gold is used to metalize the ground plane (bottom face) of the substrate with a thickness of about 200 nm and a conductivity $\sigma = 20\times10^6$ S/m at 300 GHz [13]. The fractional bandwidth of the antenna for an input reflection coefficient lower than -9 dB is larger than 50%, spanning the full frequency band from 200 GHz to 350 GHz.

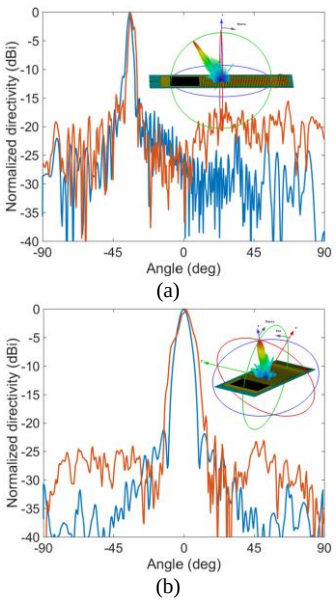

(a)

(b)

Fig. 5. Normalized directivity pattern for far-field radiation patterns at 260 GHz (red line: measured; blue line: simulated). (a) E-plane. (b) H-plane.

The blue lines in Fig. 5 depict the simulated far-field radiation patterns at the center frequency (260 GHz) in the E-plane (z-x plane in Fig. 1) and the H-plane.

Although not shown here for space limitations, the antenna scans in elevation from -76° at 220 GHz to -7° at 320 GHz. The half-power beam width (HPBW) is stable in the band of interest and ranges from 6° to 9° and from 3° to 5° in the H-plane and E-plane, respectively. The cross-polarization levels are lower than -55 dB over the full band. At higher frequencies (beyond 300 GHz), the behavior of the Luneburg lens starts to deteriorate as the sinusoidally-modulated strips do not provide the required refractive index profile. Since the H-plane is controlled by the lens, such a deterioration results in an increase of both the SLL and the HPBW in the far-field radiation patterns in that plane.

The antenna shows an average gain of 23.75 dBi with a maximum gain of 26.4 dBi at 275 GHz. The full system efficiency starts with a maximum of 40% at 220 GHz and decreases with frequency to 22% at 320 GHz. The simulated power budget of the full system at the center frequency is summarized in Table 1.

Table 2 compares our antenna with other state-of-the-art solutions at similar frequencies. A periodically loaded microstrip line is fabricated and tested in [22] to generate a fan beam. Hence, the measured gain is just 12.5 dBi. Conversely, our Luneberg lens beam-former allows one to generate a pencil beam with a single-layer structure, thus increasing the gain to 26.4 dBi. References [23]-[25] present simulation results for frequency scanning antennas. Even in simulations, the maximum reported gain is limited to 19.5 dBi at 175 GHz in [24], compared to 26.4 dBi at 275 GHz in our presented structure. This shows the complexity of the faced challenges in the sub-THz range.

Table 1. Power budget for the full structure at 260 GHz.

Directivity (dB)	Gain (dB)	Conductor Loss (dB)	Dielectric Loss (dB)	Transition Loss (dB)
31.3	26	−4.3	−1	−1.6

Table 2. Performance comparison with the prior results.

[Ref]	Freq. (GHz)	Gain (dBi)	Scanning	Fabrication
[22]	280-320	12.5	-46° - 42°	Substrate-transfer tech.
[23]	230-290	11.4	-48° - 34°	–
[24]	142-225	19.3	-68° - 60°	–
[25]	157.5–206	15	-23° - 38°	–
This work	220-290	26.4	-80° - 20°	Organic material, Photolithography based process.

IV. Experimental Results

The fabricated system is shown in Fig. 6. The lens and the array of slots are printed on the upper side of the COC substrate. First, Ti/Au (20nm/50nm) are deposited by electron beam deposition (EBD). Then, the Au layer has been thicken up to 200 nm using several evaporation steps to prevent overheating the COC. Finally, the Au layer has been patterned by photolithography, followed by chemical etching. The other side of the COC substrate (acting as a ground plane) has been also metallized using Ti/Au, as explained above, and patterned with back-side alignment photolithography. This fabrication process provides a very good accuracy (±1µm).

The supporting block with the back short for the input transition and the input waveguide has been manufactured by high-speed milling with a ±20 µm error. The COC substrate is first placed on top of the supporting block and aligned manually under a microscope. The alignment between the input waveguide in the supporting base and the flared transmission line feeding the lens is key for matching. A misalignment of about 50 µm is expected, since the substrate is too fragile for mechanical drilling and it cannot be perforated to add dowel pins (typically used for alignment). In addition, COC's low T_g does not allow one to use plasma etching or other high temperature processes for alignment holes. After the COC substrate has been carefully positioned on its supporting base, the back-short block is used as a top cover to lock the substrate

into its position. Finally, the back short and the supporting block are aligned using 2 dowel pins, and both blocks are fixed by 2 metallic screws. To further hold the substrate in place, a foam frame (white part in Fig. 6) is placed on top of the substrate and directly fixed to the supporting block with 4 Teflon screws.

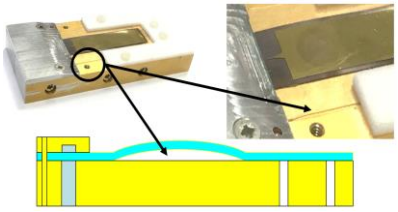

Fig. 6. Fabricated system with standard WR03 feeder on bottom and back-short on top. An external frame of foam is fixing the substrate to the holder and causing a bend in the substrate body.

The reflection coefficient and the far-field radiation patterns have been measured at IETR up to 290 GHz. The input reflection coefficient (Fig. 7) is better than −7 dB from 220 GHz to 290 GHz. The difference between the measured and the simulated results originates from two main issues. The first one is the misalignment between the waveguide block and the COC substrate. The simulated input reflection coefficient with a perfect alignment between the pre-mentioned parts is better than −9 dB over the full band. However, if the antenna system is re-simulated assuming a 50 µm misalignment, a better agreement between measured and simulated results is observed from 225 up to 265 GHz (Fig. 7). The second hurdle lies in the antenna assembly and the flexibility of the substrate. As shown in Fig. 6, the antenna is fixed by a total of 6 screws: 2 metallic screws at the beginning, and 4 at the end. Due to the pressure applied on the edges of the flexible COC structure, a bent of approximately 0.4 mm in height appeared in the middle part of the antenna (where the Luneburg lens and its feed are located). This deformation is illustrated in Fig. 6. A bent flared feeder affects the matching and the associated far-fields, since the input power may be radiated into free space directly from the feeder, without passing through the lens. Full-wave simulations taking into account such defect would require a computational effort beyond our current capabilities. However, such defect might explain the mismatch for frequencies above 265 GHz.

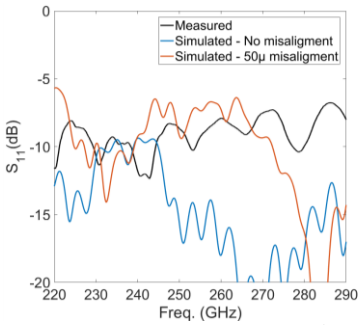

Fig. 7. Measured versus simulated magnitude of the input reflection coefficients in dB.

The far-fields radiation patterns were measured in the 2 principal planes from 220 GHz to 290 GHz with a 1 GHz step. Fig. 5 shows the measured versus simulated normalized directivity patterns in the E-plane and H-plane at 260 GHz. The agreement is considered good, although minor discrepancies can be observed for SLL lower than −15 dB. The cross-polarization level is at least 40 dB below the maximum and, thus, not plotted here.

Fig. 8 (a) shows the measured normalized directivity on the E-plane versus frequency and radiation angle. The frequency steering of the leaky-wave antenna can be clearly observed. Similarly, Fig. 8 (b) represents the measured radiation patterns along the H-plane versus frequency. It can be seen that at 270 GHz, the antenna main beam starts to split. This may be due to the bending in both the flared feeding transmission line and Luneburg lens as explained before. Nonetheless, the far-field radiation pattern along the H-plane present a SLL lower than −15 dB in the considered band.

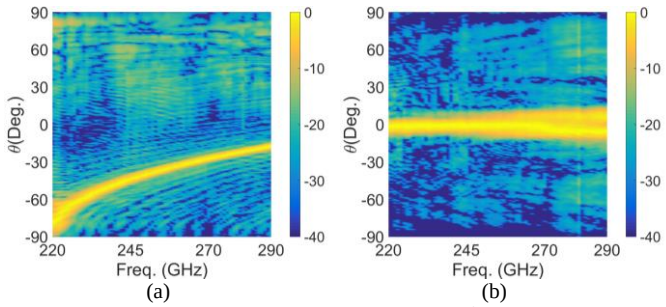

Fig. 8. Measured normalized directivity in dB versus frequency and angle. (a) E-plane. (b) H-plane.

The measured and simulated pointing angle and HPBW of the main beam along the E-plane are compared in Fig. 9. A very good agreement is observed in the steering angle between measurements and simulations, demonstrating the stability of the dielectric constant of the COC polymer in the considered frequency band. As for the HPBW, there is less than 2° deviation between simulations and measurements. This can be due to small changes in the loss tangent estimated from [17] and the conductivity of the gold layer deposited on the top and bottom sides of the structure [13]. Such changes may affect the leakage rate of the slots and the overall aperture efficiency widening the HBPW.

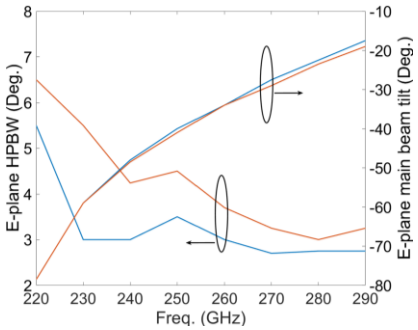

Fig. 9. Measured versus simulated main beam pointing direction and HPBW in the E-plane (red line: measured; blue line: simulated).

V. Conclusion

This letter reports the design of a polymer-based low-cost sub-THz antenna. The antenna is based on arrays of slots fed by a Luneburg lens on a COC 8007 substrate. No vias are required for the fabrication, which is a major advantage in this frequency range. The antenna is able to steer its main beam in elevation covering a field of view of about 60° in the frequency range 220-290 GHz. The total efficiency of the antenna is estimated equal to 20% at 260 GHz. Such a solution is a good candidate for low-profile, high-gain antennas at millimeter and sub-millimeter bands.

REFERENCES

[1] S. Koenig *et al*., "Wireless sub-THz communication system with high data rate," *Nature Photon.*, vol. 7, no. 12, pp. 977–981, 2013.

[2] T. S. Rappaport *et al*., "Wireless communications and applications above 100 GHz: opportunities and challenges for 6G and beyond," *IEEE Access*, vol. 7, pp. 78729-78757, 2019.

[3] H. Tataria, M. Shafi, A. F. Molisch, M. Dohler, H. Sjöland, and F. Tufvesson, "6G wireless systems: vision, requirements, challenges, insights, and opportunities," *Proc. IEEE*, vol. 109, no. 7, pp. 1166-1199, Jul. 2021.

[4] A. Hirata *et al*., "120-GHz-band wireless link technologies for outdoor 10-Gbit/s data transmission," *IEEE Trans. Microw. Theory Tech.*, vol. 60, no. 3, pp. 881–895, Mar. 2012.

[5] P. Lu *et. al*., "Mobile THz communications using photonic assisted beam steering leaky-wave antennas," *Opt. Express*, vol. 29, pp. 21629-21638, 2021.

[6] Á.J. Pascual-Gracia, *et al.*, "A photonically-excited leaky-wave antenna array at E-Band for 1-D beam steering," *Appl. Sci.*, vol. 10, pp. 3474, 2020.

[7] S. Nellen *et al*., "Photonic-enabled beam steering at 300 GHz using a photodiode-based antenna array and a polymer-based optical phased array," *Opt. Express*, vol. 30, pp. 44701-44716, 2022.

[8] D. Nüßler, "Design of a 32 element Rotman lens at 220 GHz with 20 GHz bandwidth," *German Microw. Conf.*, Nuremberg, Germany, 2015, pp. 280-283.

[9] K. Fan, Z. -C. Hao, Q. Yuan, and W. Hong, "Development of a high gain 325–500 GHz antenna using quasi-planar reflectors," *IEEE Trans. Antennas Propag.*, vol. 65, no. 7, pp. 3384-3391, Jul. 2017.

[10] M. Alonso-Delpino, T. Reck, C. Jung-Kubiak, C. Lee, and G. Chattopadhyay, "Development of silicon micromachined microlens antennas at 1.9 THz," *IEEE Trans. THz Sci. Technol.*, vol. 7, no. 2, pp. 191–198, Mar. 2017.

[11] T. J. Reck, C. Jung-Kubiak, J. Gill, and G. Chattopadhyay, "Measurement of silicon micromachined waveguide components at 500–750 GHz," *IEEE Trans. THz Sci. Technol*., vol. 4, no. 1, pp. 33–38, Jan. 2014.

[12] D. González-Ovejero, C. Jung-Kubiak, M. Alonso-del-Pino, T. Reck, and G. Chattopadhyay, "Design, fabrication and testing of a modulated metasurface antenna at 300 GHz," *Proc. 11th Eur. Conf. Antennas Propag*., Paris, France, 2017, pp. 3416-3418.

[13] K. Tekkouk *et al.*, "Corporate-feed slotted waveguide array antenna in the 350-GHz band by silicon process," *IEEE Trans. Antennas Propag.*, vol. 65, no. 1, pp. 217-225, Jan. 2017.

[14] G. Chattopadhyay *et al*., "Terahertz antennas and feeds," in *Aperture Antennas for Millimeter and Sub-Millimeter Wave Applications*, A. Boriskin, R. Sauleau, Eds. Springer, 2017.

[15] A. Mahmoud, D. González-Ovejero, M. Ettorre, and R. Sauleau, "Leaky-wave antenna array on BCB at submillimeter frequency bands," *Proc. 13th Eur. Conf. Antennas Propag*., Krakow, Poland, 2019.

[16] F. Pavanello, G. Ducournau, E. Peytavit, S. Lepilliet, and J. -F. Lampin, "High-gain Yagi–Uda antenna on Cyclic Olefin Copolymer substrate for 300-GHz applications," *IEEE Antennas Wireless Propag. Lett.*, vol. 13, pp. 939-942, 2014.

[17] I. Maestrojuan, I. Ederra, and R. Gonzalo, "Use of COC substrates for millimeter-wave devices," *Microw. Opt. Tech. Lett.*, vol. 57, no. 2, pp. 71–377, Feb. 2015.

[18] D. Cheng, "Modified Luneberg lens for defocused source," *IRE Tran. Antennas Prop*., vol. 8, no. 1, pp. 110-111, Jan. 1960.

[19] C. Pfeiffer and A. Grbic, "A printed, broadband Luneburg lens antenna," *IEEE Trans. Antennas Propag*., vol. 58, no. 9, pp. 3055–3059, Sep. 2010.

[20] Milligan, T., 2005. Modern Antenna Design. 2nd ed.

[21] CST Microwave Studio. 2022, [Online]. Available: http://www.cst.com.

[22] P. Lu et al., "InP-Based THz beam steering leaky-wave antenna," *IEEE Trans. THz Sci. Technol*, vol. 11, no. 2, pp. 218-230, March 2021.

[23] Y. Bai, and S. Liu, "A novel dual-beam terahertz leaky-wave antenna based on spoof surface plasmon waveguide," *Optoelectron. Lett.*, vol. 18, PP. 404–407, Aug. 2022.

[24] Y. Torabi, G. Dadashzadeh, A. Lalbakhsh, H. Oraizi, "High-gain and low-profile dielectric-image-line leaky-wave-antenna for wide-angle beam scanning at sub-THz frequencies," *Optics & Laser Tech*., Vol. 150, Feb. 2022.

[25] Y. Torabi, G. Dadashzadeh, M. Hadeie, H. Oraizi, and A. Lalbakhsh, "A wide-angle scanning sub-terahertz leaky-wave antenna based on a multilayer dielectric image waveguide," *Electron*., vol. 10, Feb. 2021.